

Curculigoside mitigates dextran sulfate sodium-induced colitis by activation of KEAP1-NRF2 interaction to inhibit oxidative damage and autophagy of intestinal epithelium barrier

FANG LI^{1*}, HUA HUANG^{1*}, PING ZHAO², JIE JIANG², XUFENG DING², DONXGUE LU³ and LIJIANG JI¹

Departments of ¹Digestive System and ²Anorectal Surgery, Changshu Hospital Affiliated to Nanjing University of Chinese Medicine, Changshu, Suzhou 215500; ³Department of Clinical Nutrition, Academy of Health and Rehabilitation, Academy of Acupuncture and Tuina, Nanjing University of Chinese Medicine, Nanjing, Jiangsu 210023, P.R. China

Received June 8, 2023; Accepted September 15, 2023

DOI: 10.3892/ijmm.2023.5310

Abstract. Curculigoside (CUR), a primary active ingredient of *Curculigo orchoides Gaertn.*, serves an important role in the intervention of numerous diseases, including ulcerative colitis, rheumatoid arthritis, myocardial ischemia, etc. However its specific mechanisms of therapy have not been fully elucidated. The aim of the present study was to elucidate the mechanisms underlying the anti-oxidative stress and anti-ulcerative colitis (UC) effects of CUR. Mouse model of dextran sulfate sodium (DSS)-induced colitis, along with Caco2 and mouse intestine organoid *in vitro* models were used. The effect of CUR on mitigating the symptoms of chronic colitis was investigated. Through ELISA experiments, it was observed that CUR alleviated the inflammation status in mice with chronic colitis. This was evidenced by the downregulation of inflammatory cytokines such as TNF- α and IL-6 and -1 β and decreased neutrophil infiltration along

with downregulated myeloperoxidase activity. CUR helped in maintaining the barrier functions of intestinal epithelium. *In vitro* TNF- α stimulation of organoids and H₂O₂ stimulation of Caco2 cells demonstrated the capabilities of CUR to rescue cells from oxidative stress. There was activation of Nrf2 both *in vivo* and *in vitro*, accompanied by enhanced autophagy. Mechanistic studies of cells and Nrf2 knockout mice demonstrated that Nrf2 served a pivotal role in inhibition of UC by curculigoside via interaction with Kelch-like ECH-associated protein 1 (Keap1). *In vitro* and *in vivo* experiments confirmed that CUR activated Nrf2 via Keap1/Nrf2 interaction, resulting in decreased oxidative stress and promoted autophagy. These findings demonstrated that CUR could effectively mitigate colitis and may have clinical application in UC therapy.

Introduction

Ulcerative colitis (UC), one of the two major types of inflammatory bowel disease (IBD), is widespread globally and poses notable health risks and economical burdens to human society (1). It was estimated that ulcerative colitis affected ~5 million individuals globally, with its incidence increasing globally (2). Patients with UC generally present with symptoms such as abdominal pain, bloody stool, weight loss and enterorrhea (3). Although the etiology of UC has yet to be fully elucidated yet, there are intrinsic connections between the pathogenesis and progression of UC and environment factors, intestinal barrier dysfunction and immune system disorder (4,5). Existing pharmaceutical strategies for treatment of UC have principally focused on controlling the aggravated host immune response in a broad or selective manner. Administration of biological agents, salicylates and immunomodulators results in a limited remission rate and serious side effects, including potential liver and kidney damage, in clinical practice (6). Therefore, it is imperative to identify novel strategies to intervene with UC and seek therapeutic agents with superior therapeutic efficacy.

Numerous natural products have therapeutic potential against UC and side effects are comparatively low (7,8). Curculigoside (CUR), a phenolic glycoside component of *Curculigo orchoides Gaertn.*, has been reported to alleviate

Correspondence to: Professor Donxgue Lu, Department of Clinical Nutrition, Academy of Health and Rehabilitation, Academy of Acupuncture and Tuina, Nanjing University of Chinese Medicine, 138 Xianlin, Nanjing, Jiangsu 210023, P.R. China
E-mail: 270773@njucm.edu.cn

Professor Lijiang Ji, Department of Digestive System, Changshu Hospital Affiliated to Nanjing University of Chinese Medicine, 6 Huanghe Road, Changshu, Suzhou 215500, P.R. China
E-mail: jji512@163.com

*Contributed equally

Abbreviations: CUR, curculigoside; UC, ulcerative colitis; IBD, inflammatory bowel disease; DSS, dextran sulfate sodium; ROS, reactive oxygen species; Keap1, Kelch-like ECH-associated protein 1; GSH, glutathione; MDA, malondialdehyde; SOD, superoxide dismutase; CAT, catalase; TJ, tight junction; MST, microscale thermophoresis

Key words: curculigoside, ulcerative colitis, inflammation, intestinal epithelium barrier, autophagy, Keap1, Nrf2

the symptoms of UC (9). The aim of the present study was to elucidate the mechanisms underlying the anti-oxidative stress and anti-UC effects caused by CUR.

Oxidative stress is associated with a number of diseases including UC (10). Oxidative stress results from persistent inflammation, in which high levels of reactive oxygen species (ROS) are produced from a variety of cell types (11). When the production of ROS surpasses the rate at which bowel tissue can eliminate them, ROS residues bind to specific receptors or signaling molecules associated with inflammation or cell death, including NF- κ B and caspase-dependent pathways, therefore worsening inflammation (12). This, in turn, induces apoptosis of the intestinal epithelium, causing bowel damage. Development of new means of preventing the bowel from being 'attacked' by ROS, ROS-activated cells and inflammatory cytokines secreted by activated cells during progression of UC may offer novel therapeutic strategies.

Nrf-2 is a promising target that may fulfill such an aim (13). As a crucial transcription factor, Nrf-2 maintains homeostasis at both the tissue and cellular levels by upregulating antioxidant genes (14). Attenuating the production of ROS, with the subsequent decrease in pro-inflammatory cytokine secretion in IBD, has been found to result from activation of Nrf-2 signaling (15). In addition, the role of autophagy in tissue protection and damage prevention is increasingly recognized and activation of autophagy has been developed as a strategy for treatment of various types of disease, such as cancer, polycystic ovary syndrome and osteoarthritis, among others (16–19). However, the underlying mechanism and pathway by which autophagy is activated have yet to be fully elucidated. The present study aimed to explore whether CUR induces autophagy to protect the intestine/colon.

Kelch-like ECH-associated protein 1 (Keap1) is the predominant suppressor protein of Nrf-2. The inhibition of Keap1 activity decreases the rate of degradation of Nrf-2 by the ubiquitin proteasome system, resulting in accretion of newly synthesized Nrf-2 and its translocation into the nucleus, where it triggers transcription of a series of antioxidant and cytoprotective genes, leading to the activation of cellular defense systems (20). However, the development of UC is associated with downregulation of Keap1/Nrf-2 signaling along with downstream target genes. For example, in the presence of ROS or oxidative stress, the Keap1-Nrf-2 complex sequesters inactivated Nrf-2 molecules in the cytoplasm, which are translocated to the nucleus (21). Subsequently, expression of antioxidant genes is regulated through binding of the complex to antioxidant response elements. This signal transduction process suggests that the Keap1/Nrf-2 pathway is a potential target for UC treatment (22), activation of which may prevent the detrimental effects caused by ROS on intestinal epithelium.

The present study aimed to investigate the protective function, as well as the underlying mechanisms, of CUR on UC.

Materials and methods

Chemicals and reagents. CUR (purity, $\geq 98\%$) was purchased from MedChemExpress. Fluorescein (FITC)-conjugated Affinipure donkey anti-goat IgG (cat. no. SA 079103-719) was purchased from MilliporeSigma. Zonula occludens-1 (ZO-1),

occludin, Nrf-2, microtubule-associated protein 1A/1B-light chain 3 (LC3), P62 and Beclin 1 antibodies were purchased from Cell Signaling Technology, Inc. Dextran sulfate sodium (DSS) was purchased from MP Biomedicals, LLC.

Experimental animals. A total of 30 male C57BL/6 mice (6 weeks, 20 ± 2 g) and 5 male Nrf-2^{-/-} (knockout) mice (6 weeks, 20 ± 2 g) were purchased from Labbio Biotechnology Co., Ltd. and housed at Nanjing University of Chinese Medicine. The mice were kept under conditions of $23 \pm 1^\circ\text{C}$ temperature, relative humidity 50 to 60%, and a light-dark cycle of 12 h and had ad libitum access to water and food. The animal experiments were approved by the Ethics Committee of Nanjing University of Chinese Medicine (approval no. 2022042501). Following 1 week acclimatization, the mice were randomly divided into the following groups ($n=6$ per group): Control, model (3% DSS), low- and high-dose CUR and positive control. Mice in the model group were fed 3% DSS for 8 days. C57BL/6 and Nrf-2^{-/-} mice in the low- and high-dose CUR treatment groups were administered CUR intragastrically at doses of 10 and 20 mg/kg/day, respectively, for 8 days. The positive control group was administered oral dose of 260 mg/kg/d of 5-amino-salicylic acid (5-ASA, MedChemExpress) for 8 days. The control group of mice intragastrically received an equivalent volume of normal saline. On day 9, mice were anaesthetized by intraperitoneal injection of sodium pentobarbital (50 mg/kg) and executed sacrificed by cervical dislocation.

Measurement of disease activity index (DAI). The DAI score was calculated as previously described (23). In summary, the following parameters were employed: Body weight loss (0 points, none; 1, $<5\%$; 2, 5–10%; 3, 11–20% and 4, $>20\%$), hematochezia (0 points, no bleeding; 2, slight bleeding and 4, noticeable bleeding) and diarrhea (0 points, normal stool; 2, loose stool and 4, watery diarrhea). The DAI score, which ranges from 0 to 12, was derived by combining the values of these three indicators.

Histopathological analysis. The colon tissue of mice was fixed using 4% paraformaldehyde solution at room temperature for 24 h and subsequently embedded in paraffin. The sections (5 μm) were stained with hematoxylin for 5 min and eosin for 2 min (H&E) at room temperature. Finally, histopathological changes in the colon were observed under a fluorescence microscope (Olympus, magnification, $\times 4$).

Immunofluorescence analysis. The colon tissue or cells was fixed in 4% paraformaldehyde at room temperature for 24 h. Subsequently, it was embedded in paraffin and cut into 5 μm sections. The paraffin-embedded sections were subjected to dewaxing process, involving xylene, anhydrous ethanol, 90% ethanol, 75% ethanol, and 50% ethanol. Subsequently, they were immersed in an antigen retrieval solution and a membrane permeabilization solution (cat. C1035, Solarbio Life Sciences). Finally, the sections were sealed using a neutral resin (cat. no. G8590, Solarbio Life Sciences). Slides were incubated with 5% bovine serum albumin (BSA, Dalian Meilun Biotechnology Co., Ltd.) at 37°C for 1 h and subsequently with primary antibodies targeting ZO-1 (1:200, #13663, Cell Signaling Technology) overnight at 4°C . Diluted

secondary antibodies goat anti-rabbit IgG, HRP (H+L; 1:500, cat. no. A11036, Thermo Fisher Scientific) were then added to the slides for 1 h at room temperature. Add ProLong® Gold Antifade Reagent with DAPI (#8961, Cell Signaling Technology) or Hoechst (#62249, Thermo Fisher Scientific), and incubate at room temperature in a light-protected environment for 10 min. After staining, the slides were observed under an inverted fluorescence microscope (Olympus, magnification, x4).

Permeability assay in vivo. To assess colonic permeability, FITC-dextran was employed. C57BL/6 mice received intragastric administration of FITC-dextran at a dose of 60 mg/100 g, and blood samples were collected 4 h later. The blood was left to stand in the dark for 2 h, followed by centrifugation at 1,000 g for 15 min under 4°C. Serum samples were collected and the concentration of FITC-dextran in the serum was detected at 530 nm with an excitation wavelength of 485 nm using a microplate reader.

Western blotting. Cells and tissue lysate were prepared in RIPA (Dalian Meilun Biotechnology Co., Ltd.) buffer supplemented with a proteinase inhibitor. Nuclear and cytosolic proteins were isolated following the manufacturer's instructions, utilizing the nuclear and cytosolic protein extraction kit provided by Thermo Fisher Scientific. Protein concentrations were determined using a BCA Protein Assay kit (Beyotime Institute of Biotechnology). Proteins samples (30 µg/lane) were separated by SDS-PAGE (12.5%) and electroblotted onto PVDF membranes. After blocking the membranes with 5% BSA at room temperature for 1 h, membranes were subsequently incubated with primary antibody ZO-1 (1:1,000, #13663, Cell Signaling Technology, Inc.), Occludin (1:1,000, #91131, Cell Signaling Technology), GAPDH (1:1,000, #5174, Cell Signaling Technology), Nrf2 (1:1,000, #12721, Cell Signaling Technology), Lamin B1 (1:1,000, #13435, Cell Signaling Technology) at 4°C overnight. The membranes were then washed with TBST buffer (1% Tween-20 used in TBST) three times and incubated for 1 h with secondary antibody HRP Goat Anti-Rabbit IgG (1:5,000, 9300014001, ABclonal Technology) at room temperature. Samples were washed again with TBST three times, after signals were detected using an Enhanced Chemiluminescence kit (WBKLS0100, Millipore) and ImageJ Software (version no. v1.8.0, National Institutes of Health).

Myeloperoxidase (MPO) assay. The colon tissue was homogenized for 1 min in ice-cold PBS. Subsequently, homogenates were centrifuged at 10,000 x g for 15 min at 4°C. The supernatant was collected and examined for MPO activity using the MPO ELISA kit (ab155458, Abcam) according to the manufacturer's directions.

Measurement of ROS. Flow cytometric analysis was performed for measurement of ROS levels. Cells were collected, washed with PBS and subsequently incubated with DCFDA for 30 min at 37°C in darkness. After washing twice with PBS, FITC fluorescence was analyzed by flow cytometry (Beckman CytoFlex LX) and FlowJo V.10 software (Beijing Tianyu Rongzhi Software Co.).

Measurement of colonic oxidative stress. The contents of glutathione (GSH; cat. no. E-EL-0026c, Elabscience Biotechnology, Inc.), malonaldehyde (MDA, cat. no. E-EL-0060c, Elabscience Biotechnology, Inc.), superoxide dismutase (SOD, SBJ-M0412-48T, GoldenRain/sbj) and catalase (CAT, E-BC-K031-M, Elabscience Biotechnology, Inc.) were measured in colonic tissue and cell suspensions according to the manufacturer's instructions in the commercial kit.

Determination of cytokine concentration. The concentrations of TNF-α and IL-6 and -1β in mouse colonic tissue homogenates were detected using the respective ELISA kits (cat. nos. E-EL-M3063, E-MSEL-M0001, E-EL-M0037c, Elabscience Biotechnology, Inc.), following the manufacturer's instructions.

Cell culture and treatment. Caco2 human epithelial intestinal adenocarcinoma cell line was obtained from the Cell Bank of Type Culture Collection of Chinese Academy of Sciences. Cells were cultured in a 5% CO₂, 37°C incubator in DMEM (Dalian Meilun Biotechnology Co., Ltd.) containing 10% fetal bovine serum (Gibco), 100 µg/ml streptomycin and 100 U/ml penicillin. For the H₂O₂-induced oxidative stress experiment, Caco2 cells were pre-treated with CUR (0, 30, 40 µM) for 20 h at 37°C incubator, followed by treatment with 100 µM H₂O₂ for 4 h to induce cellular oxidative stress.

Measurement of transepithelial electrical resistance (TEER). TEER of the Caco-2 cell monolayer was evaluated using the EVOM volt-ohm meter (World Precision Instruments) as previously described (24). Briefly, Caco2 cells (1x10⁵ cells/ml) were cultured at 37°C in 12-well Transwell filters with a 0.4 µm pore size for 21 days. Cells were exposed to 20 ng/ml TNF-α for 24 h at 37°C. TEER value was determined using the EVOM volt-ohm meter.

Luciferase gene reporter assay. pGL-ARE-reporter (5'-CGA GGATATTCTAGCTTGGAATGACATTGCTAATGGTG ACAAAGCAACTTTTAGCTTGGAATGACATTGCTAA TGGTGACAAAGCAACTCAAGATCTG-3') and pCWV-renilla luciferase vector (5'-CTAGCAAAATAGGCT GTCCC-3') were purchased from Genecopoeia Company. 293 cells (Cell Bank, Chinese Academy of Sciences) (1x10⁴) were seeded into 96-well plates for 12 h at 37°C. Subsequently, plasmid was transfected using Lipofectamine™ 3000 reagent (Thermo Fisher Scientific, Inc.). At 24 h post-transfection, the cells were treated with 10-40 µM CUR for 24 h. The luminescence was quantified and normalized using Nano-Glo Dual-Luciferase Reporter Assay (Promega Corporation). The luciferase activity was assessed with a Double-Luciferase Reporter Assay kit, purchased from Promega Biotech Co., Ltd., using the Dual-Light Chemiluminescent Reporter Gene Assay System, which was normalized to firefly luciferase activity.

Cellular thermal shift assay (CETSA). Cells were treated with DMSO (3 µl) and CUR (100 µM) for 1 h at 37°C and subsequently subjected to a temperature gradient (43, 46, 49, 52°C) for 3 min for each step. After heat treatment, cells were lysed (PBS supplemented with protease inhibitor (1:100, cat.

no. 87785, Thermo Fisher Scientific, Inc.) and the soluble fraction was separated by centrifugation at $16,000 \times g$ for 10 min at 4°C . The lysate was analyzed by western blotting to detect the Keap1 as aforementioned. Protein levels were quantified and the resulting melting curves were used to determine the interaction between the target and the compound in living cells.

Small interfering (si)RNA knockdown. siNrf2 (5'-GAC ATGGATTTGATTGACATACT-3') and scrambled siRNA negative control (siNC; 5'-CACTTGAATCCGACGGATTT GCA-3') were purchased from Shanghai GenePharma Co., Ltd. Caco2 cells were transfected with siNrf-2 or siNC (100 nM) for 24 h at 37°C using Lipofectamine™ 2000 transfection reagent (Thermo Fisher Scientific). On the following day, cells were exposed to the subsequent treatments. Following CUR treatment, protein expression of the siRNA target was detected by western blotting, as aforementioned.

Crypt isolation and organoid culture. Crypt isolation was performed as previously described (25). In brief, crypts were obtained from the murine small intestine by incubation for 30 min at 4°C in Dulbecco's Phosphate-Buffered Saline (D-PBS) containing 3.3 mM EDTA (Dalian Meilun Biotechnology Co., Ltd.). Isolated crypts were embedded in Matrigel, placed in 48-well culture plate and cultured in IntestCult™ OGM Mouse Basal Medium (Stemcell Technologies, Inc.) at 37°C for 7 days.

Molecular docking assay. The 3D structure of Keap1-Kelch protein complex (ID no. 3WN7) was retrieved from the Research Collaboratory for Structural Bioinformatics Protein Data Bank database (<https://www.rcsb.org/>). Autodock Tools version 4.2.6 (<https://autodock.scripps.edu/>) was used to preprocess initial protein structure, which involved removing water molecules, adding hydrogen atoms and exporting the structure to a pdbqt file for docking. The 2D structure of CUR was obtained from the PubChem database (pubchem.ncbi.nlm.nih.gov/) and converted into a Mol2 file using OpenBabel 2.3.1 (http://openbabel.org/wiki/Main_Page) software. Subsequently, hydrogen atoms were added, the charge was self-distributed and torsional construction detection was performed on the CUR structure. Docking was performed using Autodock Tools and the results were optimized using the PyMOL Molecular Graphics System software 2.4 (pymol.org/2/).

Microscale thermophoresis (MST) assay. CUR was diluted (1×10^{-9} , 4×10^{-9} , 7×10^{-9} , 10^{-8} , 4×10^{-8} , 7×10^{-8} , 10^{-7} , 4×10^{-7} , 7×10^{-7} , 10^{-6} , 4×10^{-6} , 7×10^{-6} , 1×10^{-5} , 4×10^{-5} M) using standard buffer (Tris/HCl, pH 7.4) and combined with the recombinant Keap1 protein solution (Thermo Fisher Scientific) in a 1:1 ratio. Following incubation at room temperature for 15 min, all samples were loaded into standard glass capillaries and analyzed using MST Monolith NT.115 instrument (NanoTemper Technologies GmbH) at 25°C with a laser and LED power set at 40%. The Nanotemper Analysis software (NanoTemper Technologies GmbH; version no.PR.48) was employed to calculate the dissociation constant (K_d) values.

Statistical analysis. Data are presented as the mean \pm SD (n=6). Statistical analysis was performed using GraphPad

Prism software 9.0 (Dotmatics). One-way ANOVA was used to analyze data followed by student-Newman-Keuls (three groups) or Tukey's multiple comparisons post hoc test. $P < 0.05$ was considered to indicate a statistically significant difference.

Results

CUR alleviates DSS-induced colitis in mice. The effects of CUR on attenuating UC were evaluated using a model of DSS-induced mouse colitis (Fig. 1A). Compared with the control group, DSS-induced mice had significantly shortened colons, although these symptoms were attenuated following administration of CUR and 5-ASA (Fig. 1B and C). The body weight of mice in the DSS group was significantly decreased on day 4 compared with the control group. However, in the CUR treatment and 5-ASA groups, weight loss was reversed on day 6 (Fig. 1D). Additionally, CUR and 5-ASA treatment resulted in attenuation of DSS-induced colonic tissue lesions, with DAI scores significantly lower compared with those in the DSS group (Fig. 1E). Furthermore, the regression of symptoms of colitis, including tissue damage and the inflammatory infiltration of immune cells, was observed on the basis of histological staining following CUR and 5-ASA treatment (Fig. 1F). These data demonstrated the therapeutic effects of CUR and 5-ASA on DSS-induced colitis.

Effect of CUR on inflammation of colonic tissue. Given the importance of inflammation in the pathogenesis of UC (26), the effect of CUR on inflammatory cytokine expression (TNF- α , IL-6 and IL-1 β) in colons and serum of mice with DSS-induced colitis was explored (Fig. 2A and B). Although secretion levels of TNF- α , IL-6 and IL-1 β were significantly increased in the DSS group, CUR intervention significantly reversed this trend and expression levels of these cytokines returned to normal. MPO activity is a key marker of neutrophil infiltration into colon tissue (27) and was therefore used to measure the influence of CUR on the infiltration of neutrophils. MPO activity in both the colonic tissue and serum from the DSS group was significantly higher compared with that in the control group. Following CUR intervention, however, changes in MPO activity were reversed. In conclusion, taken together, these results suggested that CUR could effectively decrease the inflammatory response in DSS-induced mice.

Effect of CUR on intestinal epithelial barrier damage in vivo and in vitro. The tight junction (TJ) is a key structure consisting of multiple protein complexes responsible for maintaining the barrier function of the intestine (28). To determine the role of CUR in the integrity of the intestinal epithelial barrier, the levels of TJ-associated proteins ZO-1 and occluding were detected using western blot and immunofluorescence assay. A significant decrease in TJ-associated proteins was observed in mouse colon tissue in the DSS group, although expression levels of these two proteins were restored in the CUR groups, indicating that CUR was able to restore the integrity of the intestinal mucosal barrier (Fig. 3A and B). Intragastric administration of FITC-dextran was used to detect intestinal permeability (Fig. 3C). CUR intervention was able to substantially prevent the increase in serum FITC-dextran in DSS mice.

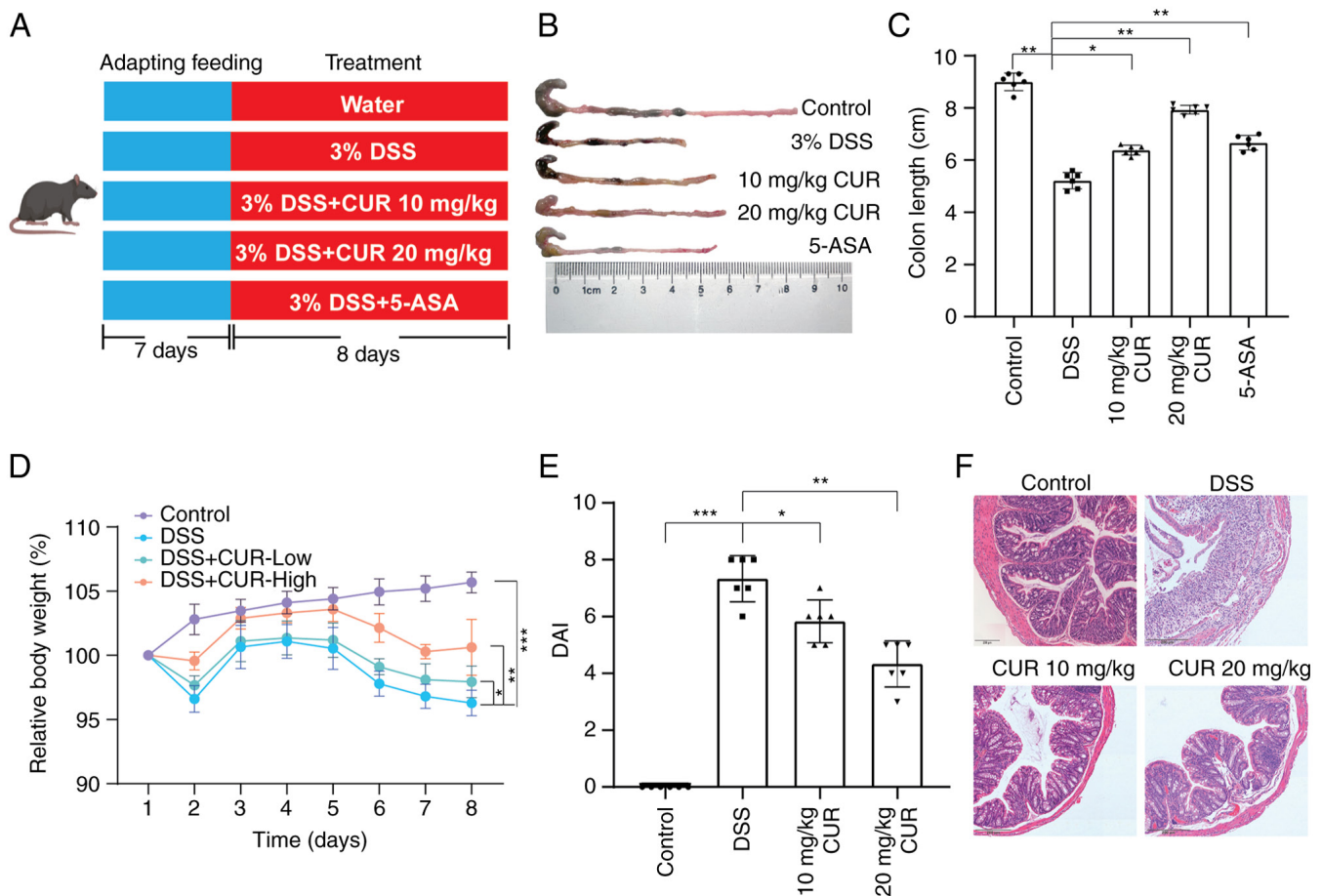


Figure 1. CUR confers protection against DSS-induced colitis in mice. (A) Animal experiment design. (B) Macroscopic inspection. (C) Colon length was detected in each group. (D) Body weight change. (E) DAI scores. (F) Colon morphology was analyzed by hematoxylin and eosin staining. Scale bar, 200 μ m. The results are representative of 6 independent experiments and expressed as the mean \pm SD. * P <0.05, ** P <0.01, *** P <0.001. CUR, curculigoside; DSS, dextran sulfate sodium; DAI, disease activity index; 5-ASA, 5-Amino salicylic acid.

To explore the effect of CUR on the properties of the TJ, expression levels of TJ marker proteins were detected and a cell barrier integrity test was performed on the TNF- α -treated Caco2 cells (Fig. 3D and E). TNF- α serves a key role in the inflammatory cascade response that induces chronic intestinal inflammation in IBD (29). Notable levels of TNF- α were secreted by mice following DSS administration (Fig. 2A). TEER was used to assess the barrier function of Caco2 cells (Fig. 3F). CUR led to a significant mitigation of the decrease in TEER induced by TNF- α . These results suggested that CUR could potentially rescue damage of intestinal barrier function in UC.

Effect of CUR on intestinal organoids following TNF- α damage. To explore the effects of CUR intervention on DSS-induced colitis, co-culture system consisting of intestinal organoids and CUR was constructed. The decrease in surface area and morphological protection of intestinal organoids induced by TNF- α were promoted following addition of CUR (Fig. 4). These results suggested that CUR promoted intestinal organoid growth.

Effect of CUR on oxidative stress in vivo and in vitro. The severity of UC depends on degree of antioxidant defense deficiency in the intestinal mucosa, which counteracts

oxidative stress in the colon that contributes to inflammatory diseases (30). DSS reduced the activity of CAT, GSH, and SOD, while increasing the activity of MAD; however, CUR effectively reversed these trends (Fig. 5A).

Hydrogen peroxide (H_2O_2) was used to induce oxidative stress in the Caco-2 cells to examine the effect and underlying mechanism of CUR intervention on oxidative stress. Significant decreases in levels of CAT, GSH and SOD were observed after treating Caco2 cells with 100 μ M H_2O_2 for 4 h. This trend, however, was reversed following CUR treatment (Fig. 5B). The levels of MDA and intracellular ROS were increased following H_2O_2 stimulation, although their levels were significantly decreased in Caco-2 cells that had been pretreated with CUR for 12 h, indicating the antioxidant activity of CUR (Fig. 5C). Furthermore, a JC-1 probe was utilized to evaluate the damage caused by matrix metalloproteinases (MMPs). H_2O_2 decreased the level of red fluorescence (JC-1 aggregate), whereas that of green fluorescence (JC-1 monomer) increased. However, CUR intervention led to a promotion of the red fluorescence, and a reduction in green fluorescence (Fig. 5D).

CUR ameliorates oxidative stress in DSS mice and H_2O_2 -treated Caco-2 cells by activating Nrf-2. Nrf-2 is a key transcription mediator involved in oxidative stress (31). Expression of Nrf-2 in mouse colonic tissue was measured

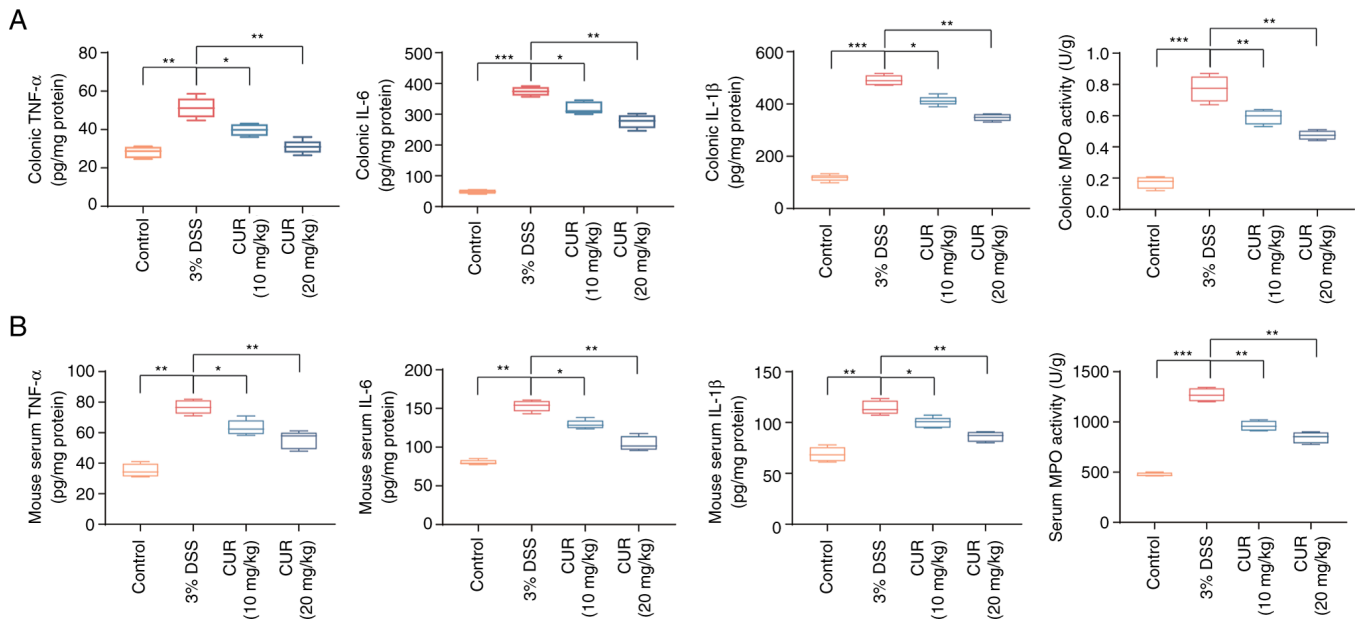


Figure 2. CUR inhibits production of proinflammatory cytokine. Protein levels of IL-1 β , IL-6, TNF- α and MPO in (A) colon and (B) serum were determined by ELISA. The results are representative of 6 independent experiments and expressed as mean \pm SD. * P <0.05, ** P <0.01, *** P <0.001. CUR, curculigoside; DSS, dextran sulfate sodium; MPO, myeloperoxidase.

using immunofluorescence and western blot assay. CUR intervention led to a significant increase in Nrf-2 (Fig. 6A and B).

Immunofluorescence assay was employed to detect the intracellular distribution of Nrf-2 in Caco-2 cells treated with control vehicle or a combination of H₂O₂ and CUR. Nrf2 was evenly localized in the cytoplasm of H₂O₂-administered Caco-2 cells, whereas the intensity of fluorescence was markedly increased in nuclei of cells treated with CUR (Fig. 6C). The effect of CUR on distribution of Nrf-2 in Caco-2 cells was further investigated using western blot assay. Following treating the Caco-2 cells with H₂O₂ for 4 h, the nuclear Nrf-2 levels were decreased, whereas pretreatment with CUR led to enhanced expression of nuclear Nrf-2 (Fig. 6D).

To determine whether CUR exerts an anti-oxidative stress effect via Nrf-2, the expression of Nrf-2 was knocked down by siRNA (Fig. S1). The contents of GSH, CAT and SOD in the H₂O₂ + CUR + siNrf-2 group were markedly decreased compared with those of the H₂O₂ + CUR group (Fig. 6E). In addition, compared with the H₂O₂ + CUR group, MDA and accumulation of ROS were found to be markedly increased in the H₂O₂ + CUR + siNrf-2 group (Fig. 6F). Consistently, the H₂O₂ + CUR + siNrf-2 group showed higher levels of MMP damage compared with the H₂O₂ + CUR group (Fig. 6G). Collectively, these data suggested that Nrf-2 promoted the influence of CUR on H₂O₂-induced oxidative stress injury.

CUR activates autophagy to protect cells via Nrf-2. Through the removal of N-acetyl-p-benzoquinone imine protein adducts or damaged mitochondria, the activation of autophagy protects tissues or organs from being damaged by oxidative stress. The present study investigated whether the presence of CUR could activate autophagy for intestine protection. The levels of autophagy markers, including LC3I, P62 and beclin-1, were detected. Under oxidative stress conditions (100 μ M H₂O₂), LC3I was upregulated in a dose-dependent

manner following administration of CUR, whereas that of the reference protein, LC3II, remained unchanged (Fig. 7A). The levels of positive regulator of autophagy beclin-1 followed a similar trend. By contrast, negative regulator of autophagy P62 was downregulated as the dose of CUR increased. Furthermore, under oxidative stress conditions, immunofluorescence staining of LC3 confirmed the dose-dependent increase in expression with changes in dose of administered CUR. Collectively, these data demonstrated that CUR activated autophagy in a dose-dependent manner, as demonstrated by the upregulation of the positive regulators of autophagy, along with downregulation of negative regulator of autophagy.

To identify through which pathway CUR activated autophagy of cells, Nrf-2 was silenced by siRNA, which was hypothesized to be the key protein to be targeted by CUR. Upregulation of the positive regulators of autophagy LC3 and P62, as well as downregulation of the negative regulator, beclin-1, were observed when Nrf-2 was silenced (Fig. 7C), which indicated that autophagy was initiated by CUR through Nrf-2 signaling under oxidative stress. Immunofluorescence further confirmed this (Fig. 7D).

Subsequently, *in vivo* experiments were performed on mice with UC. The establishment of UC induced downregulation of the autophagy-positive regulators LC3 and beclin-1 and upregulation of the negative regulator P62, suggesting that autophagy was suppressed (Fig. 7E). By contrast, CUR was found to reverse this trend in a dose-dependent manner (Fig. 7E), suggesting that it induced autophagy, thereby protecting intestine tissue from damage caused by oxidative stress.

Mitigation of UC by CUR is mediated by Nrf-2 signaling. To test the hypothesis that mitigation of UC by CUR is mediated by Nrf-2 signaling, Nrf-2^{-/-} knockout was induced in C57BL/J

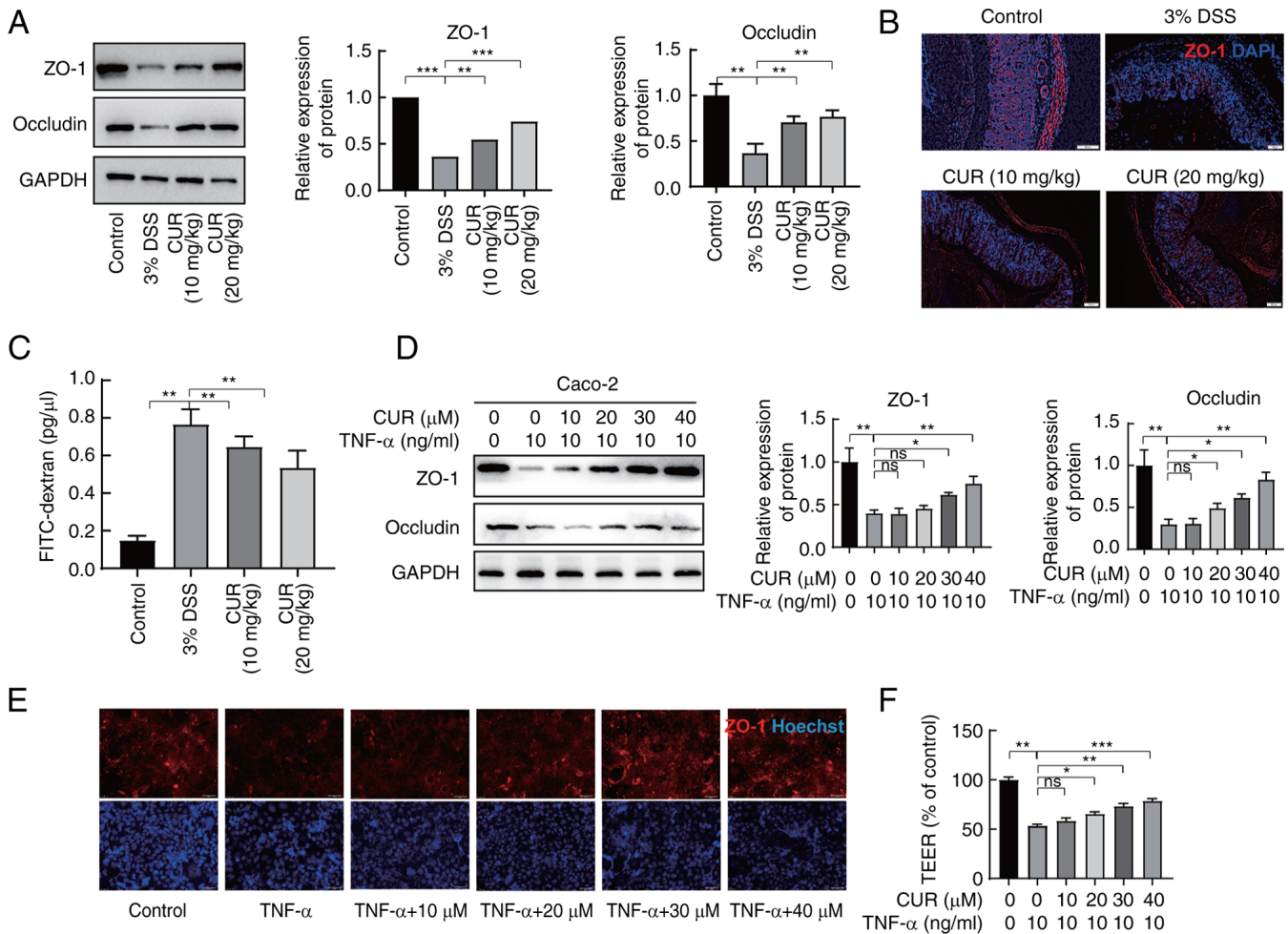


Figure 3. CUR maintains intestinal epithelial barrier integrity *in vivo* and *in vitro*. Expression of ZO-1 and occludin in colon tissue as determined by (A) western blot and (B) immunofluorescence assay. Scale bar, 100 μ m. (C) Mice were gavaged with FITC-dextran for 4 h, then serum was collected and FITC concentrations of each sample was detected. (D) Caco2 cells were treated with CUR (10, 20, 30, 40 μ M) for 4 h followed by TNF- α (100 ng/ml) for 24 h. The protein levels of ZO-1 and occludin were assessed by western blot. (E) Expression of ZO-1 in Caco2 cells was evaluated by immunofluorescence assay. Scale bar, 50 μ m. (F) Changes in the TEER value across Caco2 monolayers over time. Cells were treated with CUR prior to TNF- α . The results are representative of 6 independent experiments and expressed as the mean \pm SD. * P <0.05, ** P <0.01, *** P <0.001. CUR, curculigoside; ZO-1, Zonula occluden-1; TEER, transepithelial electrical resistance; DSS, dextran sulfate sodium.

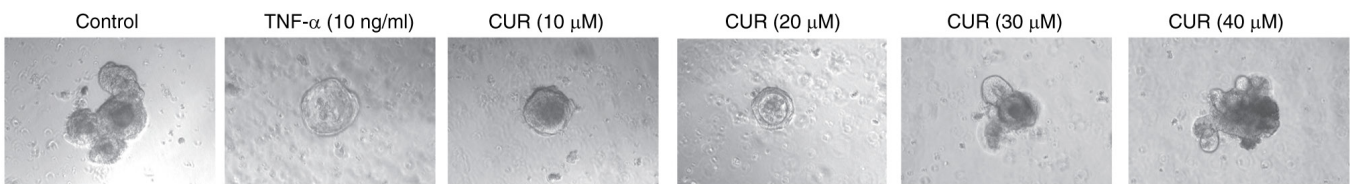


Figure 4. CUR attenuates intestinal organoid after TNF- α damage. Representative organoid images were captured at x10 magnification. Scale bar, 100 μ m. CUR, curculigoside.

mice and the effects on the amelioration of UC by CUR were explored. The severity of mouse colon damage worsened significantly with progression of UC when Nrf-2 was knockout, even in the presence of CUR. (Fig. 8A), along with a marked reduction in body weight (Fig. 8B). DAI score and HE staining of the colon indicated that Nrf-2-knockout mice experienced more severe damage during UC compared with the normal group (Fig. 8C and D). Collectively, these data suggested that the CUR protective effects on the mouse colon were mediated through Nrf-2 signaling.

CUR interferes with the interaction between Keap1 and Nrf-2 by binding to Keap1 protein. The aforementioned results demonstrated that CUR activated Nrf-2; therefore, the present study investigated whether CUR interacts with Keap1, thereby resulting in activation of Nrf-2 signaling. In the present study, CUR interacted with the target protein Keap1-Kelch. The hydroxyphenyl group of CUR formed hydrogen bonds with Val561 and Thr560 of Keap1, whereas the glucopyranoside group established hydrogen bonded with Val418 and Ile559. Additionally, the dimethoxybenzyl and hydroxyphenyl groups

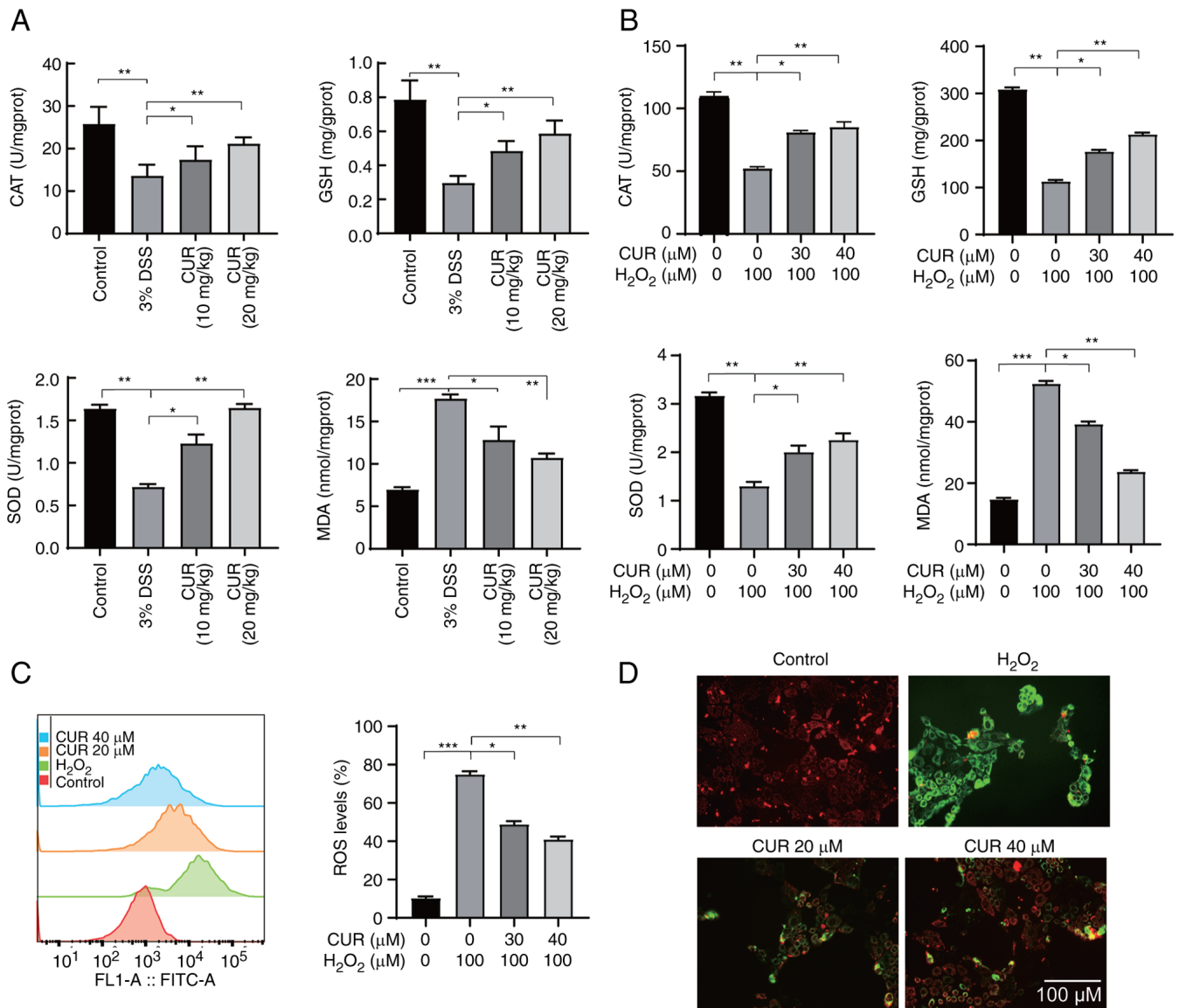


Figure 5. CUR inhibits oxidative stress *in vivo* and *in vitro*. (A) CAT, GSH, SOD and MDA in (A) mouse colon and (B) cells were detected by corresponding kits. (C) Caco2 cell ROS levels were measured by DCFHDA ROS assay kit. (D) Mitochondrial membrane potential was detected using JC-1 probe. Scale bar, 100 μm. The results are representative of 6 independent experiments and expressed as the mean ± SD. **P*<0.05, ***P*<0.01, ****P*<0.001. CUR, curculigoside; CAT, catalase; GSH, glutathione; SOD, superoxide dismutase; MDA, malondialdehyde; ROS, reactive oxygen species; DSS, dextran sulfate sodium; prot, protein.

of CUR participated in π -alkyl interactions with Val467 and Cys513 of Keap1, respectively (Fig. 9A). The binding energy of CUR with Keap1-Kelch-8.901 kcal/mol, indicating a stable interaction between the ligand and protein (Fig. 9A). In addition, luciferase reporter gene assay demonstrated that CUR activated the Nrf2, which is involved in activation of downstream antioxidant enzymes (Fig. 9B). CETSA was performed, which enables detection of the binding of small molecules to target proteins. This analysis demonstrated that the thermal stability of CUR was promoted in living Caco2 cells in the temperature range 43–52°C (Fig. 9C). Finally, the direct interaction between CUR and Keap1 was investigated using MST. Upon calibrating the binding curve using the reference compound (Fig. 9D), K_d of CUR was determined to be 4.5 μM, suggesting a strong interaction between CUR and Keap1. Taken together, this revealed that CUR directly bound to Keap1 to induce Nrf-2 activation.

Discussion

UC, one of the two primary types of IBD (the other being Crohn's disease), has been recognized as a major concern for health, resulting in major social-economic burdens for human society (32). Although conventional treatment strategies that involve suppressing inflammatory responses via administration of antibiotics are available, the limited cure rate and serious side effects associated with these therapies make the development of novel and potent alternative treatment strategies for UC an urgent need.

The present study investigated the effects of CUR in terms of relieving the symptoms of chronic colitis in a mouse UC model. Consistent with these findings, the inflammation of mice with chronic colitis was alleviated through administering CUR, as demonstrated by downregulated expression of a number of inflammatory cytokines,

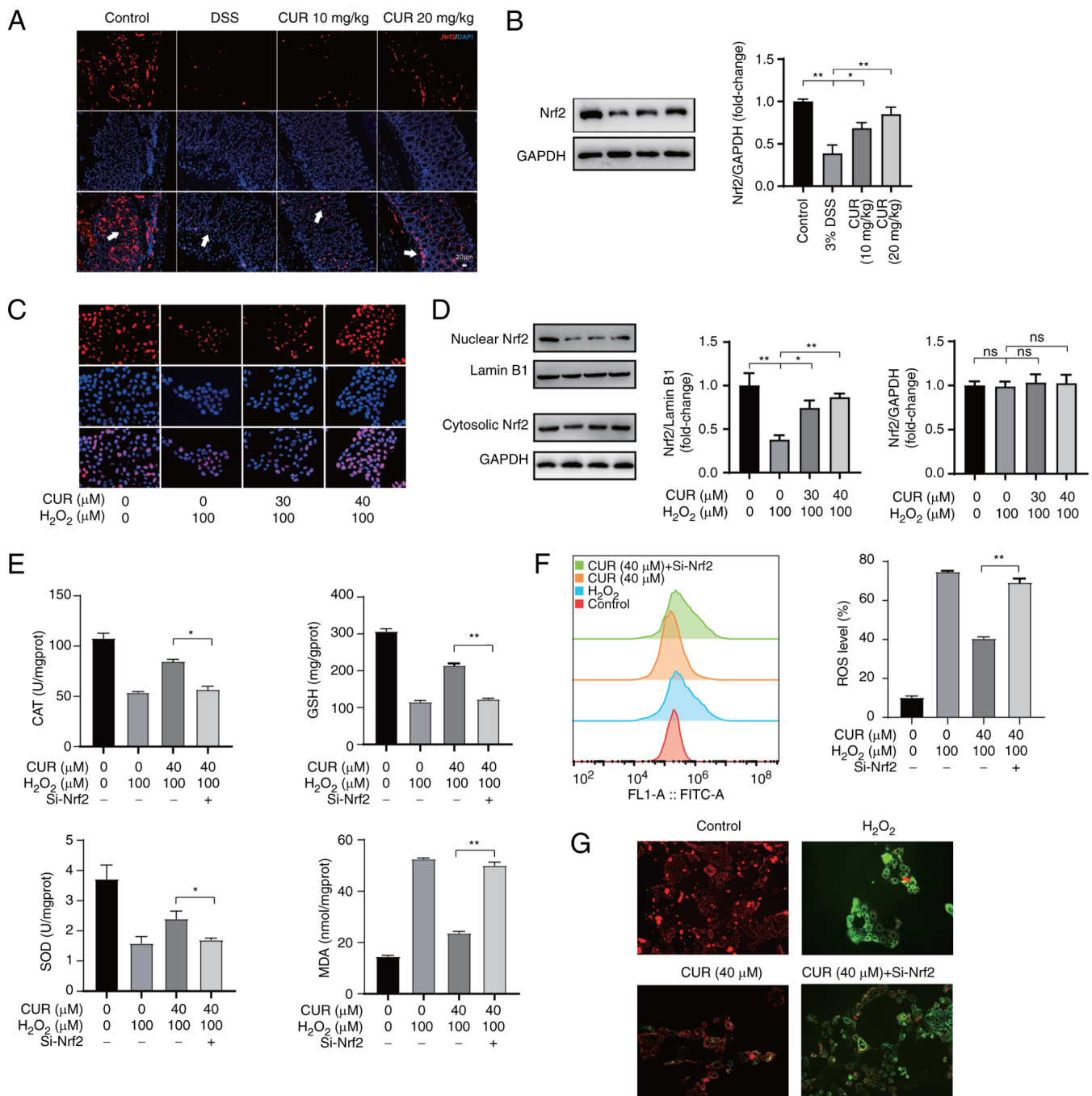


Figure 6. CUR relieves oxidative stress in DSS-administrated mice and H₂O₂-treated Caco-2 cells by activating Nrf-2. (A) Nrf-2 (arrow) distribution in mouse colon was measured using immunofluorescence. (The arrowhead represents Nrf-2 expression). Scale bar, 20 μm. (B) Western blot was used to determine expression of Nrf-2. (C) Nrf-2 distribution in cells was measured using immunofluorescence. Scale bar, 100 μm. (D) Expression of Nrf-2 in cytosolic and nuclear extract was determined by western blot. Lamin B1 and GAPDH were used as nuclear and cytoplasmic markers, respectively (E) Following Nrf2 siRNA transfection, Caco2 cells were treated with CUR for 24 h followed by H₂O₂ stimulation for 4 h. CAT, GSH, SOD and MDA were detected by corresponding kits. (F) ROS was evaluated by spectrofluorometer. (G) Mitochondrial membrane potential was determined by JC-1 probe. Scale bar, 100 μm. The results are representative of 6 independent experiments and expressed as the mean ± SD. *P<0.05, **P<0.01. CUR, curcumin; DSS, dextran sulfate sodium; si, small interfering; CAT, catalase; GSH, glutathione; SOD, superoxide dismutase; MDA, malondialdehyde; prot, protein.

including TNF-α, IL-6 and IL-1β, decreased neutrophil infiltration and downregulated MPO activity. Furthermore, CUR helped to maintain the barrier functions of the intestinal epithelium. In addition, *in vitro* organoid and Caco2 cell experiments demonstrated the capabilities of CUR in terms of rescuing cells from oxidative stress. CUR could promote the autophagy of cells under conditions of oxidative stress through Nrf-2 signaling and autophagy promoted the ability

of CUR to protect the colon tissue from damage by oxidative stress. Mechanistic studies demonstrated that activation of Nrf-2 served a pivotal role in inhibition of UC by CUR. This hypothesis was confirmed using an Nrf-2 knockout mouse and interaction of CUR with protein Keap1/Kelch. 5-ASA, also known as mesalazine is a first-line drug for treatment of inflammatory bowel diseases such as UC, with a high effective rate of induction and maintenance of remission.

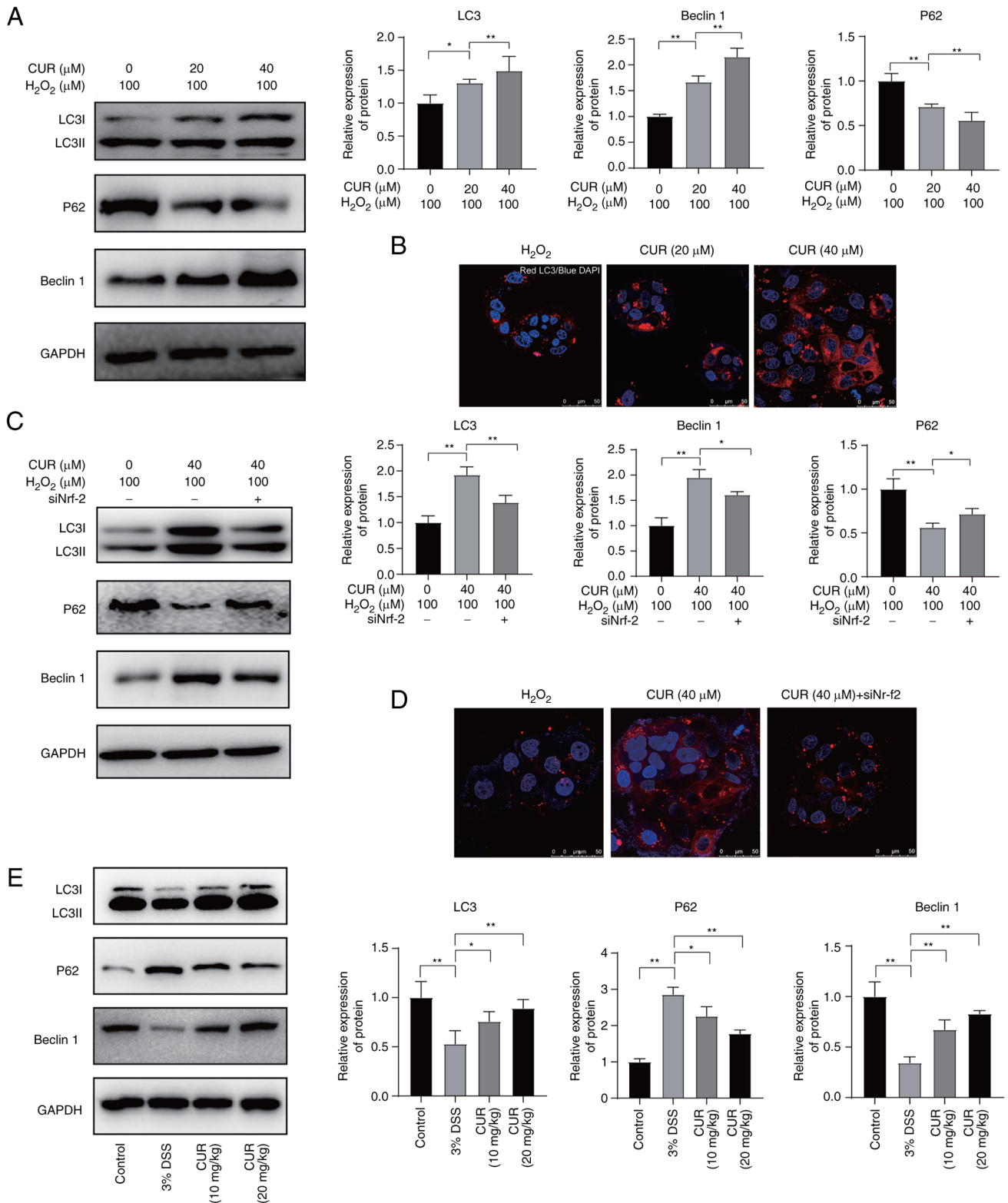


Figure 7. CUR regulates autophagy by activating Nrf-2. (A) Caco2 cells were treated with H₂O₂ or CUR + H₂O₂. Western blot was used to measure the protein expression of LC3I/II, P62 and Beclin 1. (B) Immunofluorescence images of LC3I/II. LC3I/II was marked using CY3 red immunofluorescence and nuclei were labeled using Hoechst. Scale bar, 50 μm. (C) After Nrf2 siRNA transfection, Caco2 cells were treated with CUR for 24 h followed by H₂O₂ stimulation for 4 h. Western blot was used to measure protein expression of LC3I/II, P62 and Beclin 1. (D) Immunofluorescence images of LC3I/II. Scale bar, 50 μm. (E) Protein expression of LC3I/II, P62 and Beclin 1 in mouse colonic tissue was determined by western blot. The results are representative of 6 independent experiments and expressed as the mean ± SD. *P<0.05, **P<0.01. CUR, curculigoside; si, small interfering; DSS, dextran sulfate sodium

It has antioxidant activity and decreases tissue damage. 5-ASA is important for prevention of T cell activation and proliferation. It negatively regulates the cyclooxygenase

and lipoxygenase pathways and decreases production of prostaglandins and leukotrienes (33). Therefore 5-ASA was used as a positive drug for comparison.

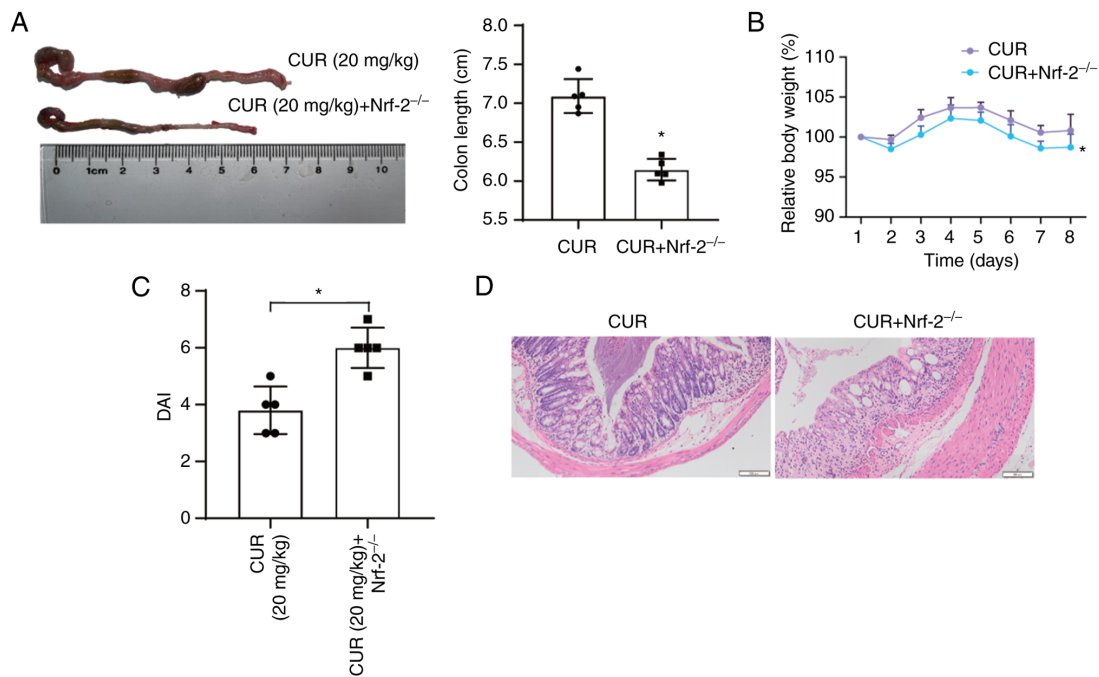


Figure 8. CUR does not exert a therapeutic role in DSS-induced colitis Nrf-2^{-/-} mice. (A) Macroscopic inspection and colon length was detected. (B) Relative body weight. (C) DAI scores. (D) Colon morphology was analyzed by hematoxylin and eosin staining. Scale bar, 100 μ m. The results are representative of six independent experiments and expressed as the mean \pm SD. *P<0.05. CUR, curculigoside; DSS, dextran sulfate sodium; DAI, disease activity index.

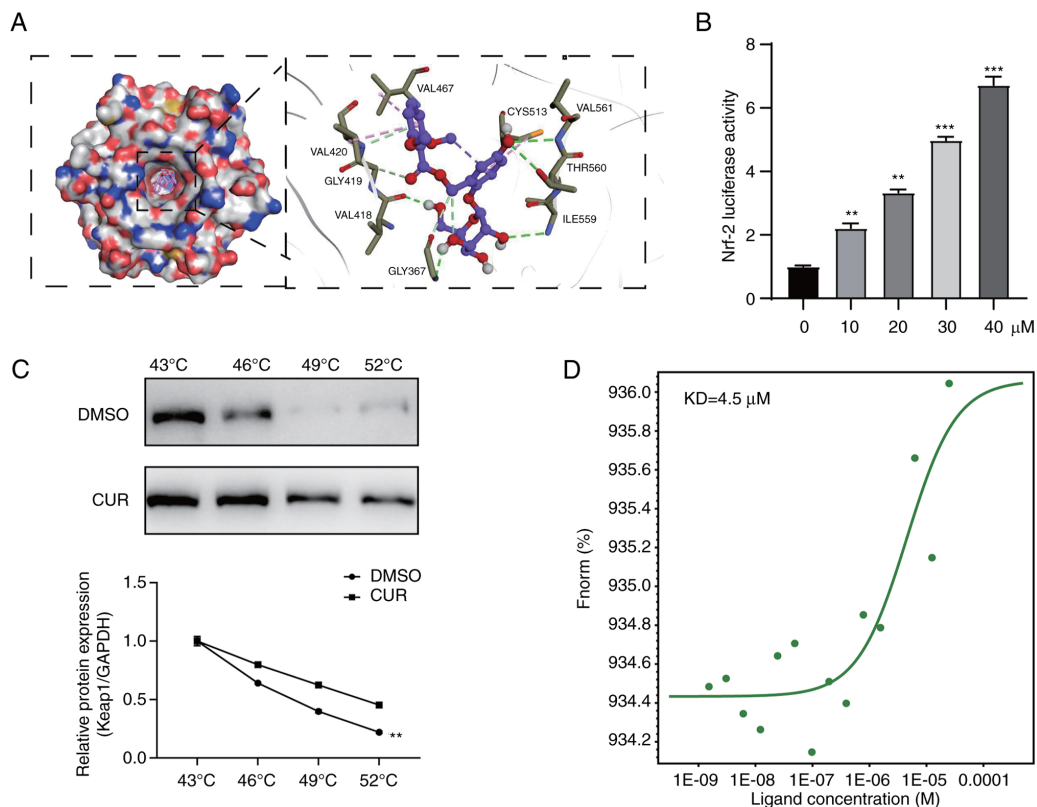


Figure 9. CUR interferes with the interaction between Keap1 and NRF-2 by binding to Keap1 protein. (A) Ligand docking analysis for CUR with human Keap1 protein. (B) Nrf-2 activity was determined using Luciferase reporter gene. (C) Western blot for Keap1 in whole cell lysate from Caco2 incubated in the presence or absence of 10 μ M Caco2. (D) Measurement of binding affinity of CUR with KEAP1 by MST. The results are representative of six independent experiments and expressed as the mean \pm SD. Compared with control group, **P<0.01, ***P<0.001 vs. control. CUR, curculigoside; Keap1, Kelch-like ECH-associated protein 1; MST, microscale thermophoresis; KD, dissociation constant; F_{norm}, normalized fluorescence.

As a natural phenolic glycoside compound, CUR has been shown to inhibit the progression of various types of diseases (34,35); furthermore, it promotes tissue regeneration, including osteogenesis, and modulates immune

responses (36). In the present study, the therapeutic effect of CUR on UC via modulating interaction of Keap1/Nrf-2 in the Nrf-2 signaling pathway was demonstrated. The results were consistent with those of a previous study in terms of the protective effects of CUR on UC (9), although the aforementioned study focused on the protective effects of CUR on ferroptosis in UC.

To the best of our knowledge, the present study is the first to demonstrate the role of Nrf-2 and Keap1 on the therapeutic effects of CUR on UC. Keap1 is the primary negative modulator of Nrf-2, which regulates the steady-state levels of Nrf-2 under diverse intracellular redox states (37). The role of Nrf-2 activation in inflammation suppression has been investigated in a variety of diseases. For example, Huang *et al* (38) demonstrated the role of Nrf-2 activation in the attenuation of lung injury and resultant oxidative stress. Wu *et al* (39) reported that the interaction of Keap1/Nrf2 with the natural product acacetin alleviates myocardial ischemia/reperfusion injury. Other examples include the therapeutic effects of sleep deprivation-induced neuroinflammation (40), cardiovascular injury (41) and different types of cancer (42,43). These reports demonstrated the effects of Nrf-2 activation on treatment of diseases associated with inflammation.

In addition, ROS elimination or depletion stimulates Nrf-2 activation; this has been investigated in the treatment of the aforementioned diseases (44). In the present study, DSS led to a notable decrease in the activities of CAT, GSH and SOD, indicating the loss of the antioxidant enzyme defense system; CUR, however, effectively reversed these trends. In addition, compared with the H₂O₂ + CUR group, MDA and ROS accumulation were markedly increased in the H₂O₂ + CUR + siNrf-2 group.

To protect the body from peroxidative damage, cells form a complex antioxidant enzyme defense system, primarily comprising SOD, CAT and GSH, in which SOD converts toxic superoxide anion into H₂O₂ and CAT converts H₂O₂ into water. CAT is also able to regulate levels of H₂O₂, in addition to acting as a protective agent of hemoglobin and other sulfhydryl proteins (45). Reduced GSH is oxidized to glutathione disulfide (GSSG) and the ratio of GSH to GSSG in cells provides a measure of cellular oxidative stress (46). In the present study, downregulation of levels of SOD, CAT and GSH suggested that the activity of the antioxidant enzyme system induced by bowel inflammation was suppressed, whereas this trend was reversed upon administering CUR, indicating recovery of the activity of the antioxidant enzyme defense system. In addition, MAD is a lipid peroxidation metabolite commonly used as a marker to measure lipid peroxidation metabolism *in vivo*, serving as an indicator to assess the generation of free radicals and damage they cause to the structure of the membrane lipid bilayer (47). In the present study, downregulation of MAD following CUR administration demonstrated elimination of oxidative stress mediated by CUR that occurred during inflammation. These data highlighted the therapeutic effect of CUR in terms of eliminating ROS, suggesting its potential clinical utility. Future studies should investigate the protective effects of CUR on local tissue and organs in other types of disease involving increased oxidative stress either locally

or systematically, regardless of whether oxidative stress acts as the upstream regulator or downstream effector.

In conclusion, CUR is potentially a potent therapeutic compound for UC that is able to activate Nrf-2 signaling, as demonstrated both in an animal model and in *in vitro* cell and organoid models. The molecular docking simulation demonstrated that CUR targeted the interaction of Keap1 and Nrf-2. Taken together, these data confirmed the therapeutic effects of CUR on UC and the underlying mechanism. These findings may facilitate the clinical application of CUR in UC therapy.

Acknowledgements

Not applicable.

Funding

The present study was supported by Jiangsu Traditional Chinese Medicine Science and Technology Development Project (grant no. MS2021058); Natural Science Foundation of Nanjing University of Chinese Medicine (grant no. XZR2020062); Suzhou Municipal Science and Technology Bureau Supporting Project (grant no. SKY2022072); Changshu Municipal Science and Technology Bureau Supporting Project (grant nos. CS202233 and CS202030) and Open Project of Zhenjiang Traditional Chinese Medicine Spleen and Stomach Diseases Clinical Medicine Research Center (grant no. SSPW2022-KF08).

Availability of data and materials

The datasets used and analyzed during the current study are available from the corresponding author on reasonable request.

Authors' contributions

LJ designed and performed the experiments, analyzed data and edited the manuscript. DL performed the experiments and wrote and edited the manuscript. FL designed the experiments and analyzed data. HH designed and performed the experiments and analyzed data. PZ and XD designed the experiments. JJ performed the experiments and wrote and edited the manuscript. All authors have read and approved the final manuscript. LJ and JJ confirm the authenticity of all the raw data.

Ethics approval and consent to participate

Ethics approval for animal experiments was received from the Experimental Animal Ethics Committee of Nanjing University Of Chinese Medicine (approval no. 2022053209).

Patient consent for publication

Not applicable.

Competing interests

The authors declare that they have no competing interests.

References

- Thorsteinsdottir S, Gudjonsson T, Nielsen OH, Vainer B and Seidelin JB: Pathogenesis and biomarkers of carcinogenesis in ulcerative colitis. *Nat Rev Gastroenterol Hepatol* 8: 395-404, 2011.
- Le Berre C, Honap S and Peyrin-Biroulet L: Ulcerative colitis. *Lancet* 402: 571-584, 2023.
- Aarestrup J, Jess T, Kobylecki CJ, Nordestgaard BG and Allin KH: Cardiovascular risk profile among patients with inflammatory bowel disease: A population-based study of more than 100 000 individuals. *J Crohns Colitis* 13: 319-323, 2019.
- Larabi A, Barnich N and Nguyen HT: New insights into the interplay between autophagy, gut microbiota and inflammatory responses in IBD. *Autophagy* 16: 38-51, 2020.
- Nikolaus S and Schreiber S: Diagnostics of inflammatory bowel disease. *Gastroenterology* 133: 1670-1689, 2007.
- Zhao J, Gao W, Cai X, Xu J, Zou D, Li Z, Hu B and Zheng Y: Nanozyme-mediated catalytic nanotherapy for inflammatory bowel disease. *Theranostics* 9: 2843-2855, 2019.
- Huang S, Fu Y, Xu B, Liu C, Wang Q, Luo S, Nong F, Wang X, Huang S, Chen J, *et al*: Wogonoside alleviates colitis by improving intestinal epithelial barrier function via the MLCK/pMLC2 pathway. *Phytomedicine* 68: 153179, 2020.
- Zhong Y, Liu W, Xiong Y, Li Y, Wan Q, Zhou W, Zhao H, Xiao Q and Liu D: Astragaloside IV alleviates ulcerative colitis by regulating the balance of Th17/Treg cells. *Phytomedicine* 104: 154287, 2022.
- Wang S, Liu W, Wang J and Bai X: Curculigoside inhibits ferroptosis in ulcerative colitis through the induction of GPX4. *Life sci* 259: 118356, 2020.
- Elmaksoud HAA, Motawea MH, Desoky AA, Elharrif MG and Ibrahim A: Hydroxytyrosol alleviate intestinal inflammation, oxidative stress and apoptosis resulted in ulcerative colitis. *Biomed Pharmacother* 142: 112073, 2021.
- Roessner A, Kuester D, Malfertheiner P and Schneider-Stock R: Oxidative stress in ulcerative colitis-associated carcinogenesis. *Pathol Res Pract* 204: 511-524, 2008.
- Colombo BB, Fattori V, Guazelli CFS, Zaninelli TH, Carvalho TT, Ferraz CR, Bussmann AJC, Ruiz-Miyazawa KW, Baracat MM, Casagrande R and Verri WA Jr: Vinpocetine ameliorates acetic acid-induced colitis by inhibiting NF- κ B activation in mice. *Inflammation* 41: 1276-1289, 2018.
- Torrente L and DeNicola GM: Targeting NRF2 and its downstream processes: Opportunities and challenges. *Annu Rev Pharmacol Toxicol* 62: 279-300, 2022.
- Liu S, Pi J and Zhang Q: Signal amplification in the KEAP1-NRF2-ARE antioxidant response pathway. *Redox Biol* 54: 102389, 2022.
- Bauer C, Dueswell P, Mayer C, Lehr HA, Fitzgerald KA, Dauer M, Tschopp J, Endres S, Latz E and Schnurr M: Colitis induced in mice with dextran sulfate sodium (DSS) is mediated by the NLRP3 inflammasome. *Gut* 59: 1192-1199, 2010.
- Cai X, Hua S, Deng J, Du Z, Zhang D, Liu Z, Khan NU, Zhou M and Chen Z: Astaxanthin activated the Nrf2/HO-1 pathway to enhance autophagy and inhibit ferroptosis, ameliorating acetaminophen-induced liver injury. *ACS Appl Mater Interfaces* 14: 42887-42903, 2022.
- Gao K, Shi Q, Liu Y and Wang C: Enhanced autophagy and NFE2L2/NRF2 pathway activation in SPOP mutation-driven prostate cancer. *Autophagy* 18: 2013-2015, 2022.
- Debnath J, Gammoh N and Ryan KM: Autophagy and autophagy-related pathways in cancer. *Nat Rev Mol Cell Bio* 24: 560-575, 2023.
- Kumariya S, Ubba V, Jha RK and Gayen JR: Autophagy in ovary and polycystic ovary syndrome: Role, dispute and future perspective. *Autophagy* 17: 2706-2733, 2021.
- Gao Z, Yi W, Tang J, Sun Y, Huang J, Lan T, Dai X, Xu S, Jin ZG and Wu X: Urolithin A protects against acetaminophen-induced liver injury in mice via sustained activation of Nrf2. *Int J Biol Sci* 18: 2146-2162, 2022.
- Negrette-Guzmán M, Huerta-Yepez S, Tapia E and Pedraza-Chaverri J: Modulation of mitochondrial functions by the indirect antioxidant sulforaphane: A seemingly contradictory dual role and an integrative hypothesis. *Free Radical Bio Med* 65: 1078-1089, 2013.
- Piotrowska M, Swierczynski M, Fichna J and Piechota-Polanczyk A: The Nrf2 in the pathophysiology of the intestine: Molecular mechanisms and therapeutic implications for inflammatory bowel diseases. *Pharmacol Res* 163: 105243, 2021.
- Wirtz S, Neufert C, Weigmann B and Neurath MF: Chemically induced mouse models of intestinal inflammation. *Nat Protoc* 2: 541-546, 2007.
- Corpetti C, Del Re A, Seguela L, Palencia I, Rurgo S, De Conno B, Pesce M, Sarnelli G and Esposito G: Cannabidiol inhibits SARS-Cov-2 spike (S) protein-induced cytotoxicity and inflammation through a PPAR γ -dependent TLR4/NLRP3/Caspase-1 signaling suppression in Caco-2 cell line. *Phytother Res* 35: 6893-6903, 2021.
- Geng H, Bu HF, Liu F, Wu L, Pfeifer K, Chou PM, Wang X, Sun J, Lu L, Pandey A, *et al*: In inflamed intestinal tissues and epithelial cells, interleukin 22 signaling increases expression of H19 long noncoding RNA, which promotes mucosal regeneration. *Gastroenterology* 155: 144-155, 2018.
- Podolsky DK: Inflammatory bowel disease. *New Engl J Med* 347: 417-429, 2002.
- Wu Y, Jha R, Li A, Liu H, Zhang Z, Zhang C, Zhai Q and Zhang J: Probiotics (Lactobacillus plantarum HNU082) supplementation relieves ulcerative colitis by affecting intestinal barrier functions, immunity-related gene expression, gut microbiota, and metabolic pathways in mice. *Microbiol Spectr* 10: e165122, 2022.
- Foerster EG, Mukherjee T, Cabral-Fernandes L, Rocha JDB, Girardin SE and Philpott DJ: How autophagy controls the intestinal epithelial barrier. *Autophagy* 18: 86-103, 2022.
- Michielan A and D'Inca R: Intestinal permeability in inflammatory bowel disease: Pathogenesis, clinical evaluation, and therapy of leaky gut. *Mediat Inflamm* 2015: 628157, 2015.
- Perico L, Morigi M, Rota C, Breno M, Mele C, Noris M, Introna M, Capelli C, Longaretti L, Rottoli D, *et al*: Human mesenchymal stromal cells transplanted into mice stimulate renal tubular cells and enhance mitochondrial function. *Nat Commun* 8: 983, 2017.
- Tang Z, Hu B, Zang F, Wang J, Zhang X and Chen H: Nrf2 drives oxidative stress-induced autophagy in nucleus pulposus cells via a Keap1/Nrf2/p62 feedback loop to protect intervertebral disc from degeneration. *Cell Death Dis* 10: 510, 2019.
- Ghafouri-Fard S, Eghtedarian R and Taheri M: The crucial role of non-coding RNAs in the pathophysiology of inflammatory bowel disease. *Biomed Pharmacother* 129: 110507, 2020.
- Le Berre C, Roda G, Nedeljkovic PM, Danese S and Peyrin-Biroulet L: Modern use of 5-aminosalicylic acid compounds for ulcerative colitis. *Expert Opin Biol Ther* 20: 363-378, 2020.
- Guo H, Zheng L, Guo Y, Han L, Yu J and Lai F: Curculigoside represses the proliferation and metastasis of osteosarcoma via the JAK/STAT and NF- κ B signaling pathways. *Biol Pharm Bull* 45: 1466-1475, 2022.
- Han J, Wan M, Ma Z, Hu C and Yi H: Prediction of targets of curculigoside A in osteoporosis and rheumatoid arthritis using network pharmacology and experimental verification. *Drug Des Devel Ther* 14: 5235-5250, 2020.
- Shen Q, Zeng D, Zhou Y, Xia L, Zhao Y, Qiao G, Xu L, Liu Y, Zhu Z and Jiang X: Curculigoside promotes osteogenic differentiation of bone marrow stromal cells from ovariectomized rats. *J Pharm Pharmacol* 65: 1005-1013, 2013.
- Yamamoto M, Kensler TW and Motohashi H: The KEAP1-NRF2 system: A thiol-based sensor-effector apparatus for maintaining redox homeostasis. *Physiol Rev* 98: 1169-1203, 2018.
- Huang CY, Deng JS, Huang WC, Jiang WP and Huang GJ: Attenuation of lipopolysaccharide-induced acute lung injury by hispolon in mice, through regulating the TLR4/PI3K/Akt/mTOR and Keap1/Nrf2/HO-1 pathways, and suppressing oxidative stress-mediated ER stress-induced apoptosis and autophagy. *Nutrients* 12: 1742, 2020.
- Wu C, Chen RL, Wang Y, Wu WY and Li G: Acacetin alleviates myocardial ischaemia/reperfusion injury by inhibiting oxidative stress and apoptosis via the Nrf-2/HO-1 pathway. *Pharm Biol* 60: 553-561, 2022.
- Xue R, Wan Y, Sun X, Zhang X, Gao W and Wu W: Nicotinic mitigation of neuroinflammation and oxidative stress after chronic sleep deprivation. *Front Immunol* 10: 2546, 2019.
- Zou L, Liang B, Gao Y, Ye T, Li M, Zhang Y, Lu Q, Hu X, Li H, Yuan Y and Xing D: Nicotinic acid riboside regulates Nrf-2/P62-related oxidative stress and autophagy to attenuate doxorubicin-induced cardiomyocyte injury. *Biomed Res Int* 2022: 6293329, 2022.
- Nair N and Gongora E: Oxidative stress and cardiovascular aging: Interaction between NRF-2 and ADMA. *Curr Cardiol Rev* 13: 183-188, 2017.

43. Nazmeen A, Chen G and Maiti S: Dependence between estrogen sulfotransferase (SULT1E1) and nuclear transcription factor Nrf-2 regulations via oxidative stress in breast cancer. *Mol Biol Rep* 47: 4691-4698, 2020.
44. Xu J, Chu T, Yu T, Li N, Wang C, Li C, Zhang Y, Meng H and Nie G: Design of diselenide-bridged hyaluronic acid nano-antioxidant for efficient ROS scavenging to relieve colitis. *Acs Nano* 16: 13037-13048, 2022.
45. Moniruzzaman M, Ghosal I, Das D and Chakraborty SB: Melatonin ameliorates H₂O₂-induced oxidative stress through modulation of Erk/Akt/NFκB pathway. *Biol Res* 51: 17, 2018.
46. Giustarini D, Dalle-Donne I, Milzani A, Fanti P and Rossi R: Analysis of GSH and GSSG after derivatization with N-ethylmaleimide. *Nat Protoc* 8: 1660-1669, 2013.
47. Tan SC, Rajendran R, Bhattamisra SK, Krishnappa P, Davamani F, Chitra E, Ambu S, Furman B and Candasamy M: Effect of madecassoside in reducing oxidative stress and blood glucose in streptozotocin-nicotinamide-induced diabetes in rats. *J Pharm Pharmacol* 75: 1034-1045, 2023.



Copyright © 2023 Li et al. This work is licensed under a Creative Commons Attribution-NonCommercial-NoDerivatives 4.0 International (CC BY-NC-ND 4.0) License.